Arabian Journal of Chemistry (2022) **15**, 104364

King Saud University

Arabian Journal of Chemistry

www.ksu.edu.sa
www.sciencedirect.com

ORIGINAL ARTICLE

Experimental and theoretical evaluation of synthetized cobalt oxide for phenol adsorption: Adsorption isotherms, kinetics, and thermodynamic studies

Adil Lammini [a], Ali Dehbi [a], Hind Omari [a], Kaoutar ELazhari [a], Smahane Mehanned [b], Youssera Bengamra [a], Younes Dehmani [a,*], Oukhrib Rachid [c], Awad A. Alrashdi [d], Obey Gotore [e], Abdelaziz Abdellaoui [a], Hassane Lgaz [f,*]

[a] *Laboratory of Applied Physical Chemistry Ability of Sciences, 4010, BeniM'Hamed, Meknes, Morocco*
[b] *Department of Biology, Faculty of Sciences, Moulay Ismail University, B.P. 11201 Zitoune, Meknes, Morocco*
[c] *Applied Chemistry-Physics Team, Faculty of Sciences, Ibn Zohr University, Agadir, Morocco*
[d] *Chemistry Department, Umm Al-Qura University, Al-Qunfudah University College, Saudi Arabia*
[e] *Graduate School of Engineering, Nagasaki University, 852-8521 Nagasaki, Japan*
[f] *Innovative Durable Building and Infrastructure Research Center, Center for Creative Convergence Education, Hanyang University ERICA, 55 Hanyangdaehak-ro, Sangrok-gu, Ansan-si, Gyeonggi-do 15588, Republic of Korea*

Received 15 June 2022; accepted 11 October 2022
Available online 18 October 2022

KEYWORDS

Cobalt oxide;
Phenol;
Adsorption;
DFT;
MD

Abstract Water pollution by phenolic composites is considered a major environmental problem. Therefore, their removal by adsorption is of great practical importance. In this paper, the synthesized cobalt oxide Co_3O_4 was used as an adsorbent for the adsorption of phenol in an aqueous medium. A DFT calculation has been carried out to determine the sites accountable for the interactions in phenol molecule, and molecular dynamics (MD) simulations were used to understand the mechanism of interaction between phenol molecule and Co_3O_4 surface. The developed adsorbent was characterized by physicochemical methods including XRD, SEM, FT-IR, and BET. The maximum adsorption capacity was observed at pH = 4 with an adsorbed amount of 8.10 mg/g and (R = 98 %). Furthermore, to probe the adsorption action of the phenolic emulsion on the cobalt oxide face, theoretical simulations based on MD (molecular dynamics) and DFT (viscosity functional proposal) were performed. The DFT results verified the chemisorption ascendancy while

* Corresponding authors.
E-mail addresses: dehmaniy@gmail.com (Y. Dehmani), hlgaz@hanyang.ac.kr (H. Lgaz).
Peer review under responsibility of King Saud University.

Production and hosting by Elsevier

https://doi.org/10.1016/j.arabjc.2022.104364

the MD simulations indicated an increased trade of Co_3O_4 with phenol in the presence of detergent due to water-bridged H- bonds.

1. Introduction

Globally, wastewater treatment is the number one public health issue. Wastewater contains many harmful substances that become from industrial activities, and agricultural and household waste. Assessing and managing the risks of the presence of harmful chemicals in the ecosystem is a needed way that integrates different skills in the environmental field. Although much energy has been invested in wastewater treatment, unfortunately, it is estimated that there is still a lot of liquid discharge today to the treatment plant; the rest is discharged into the natural environment (Ba Mohammed, 2019). The problem of not having clear policies or proper treatment systems will increase the pollution of industrial wastewater which can reduce the concentration of pollutants discharged into the plant. Naturally, this will inevitably lead to a decline in water quality, especially in many countries with a shortage of drinking water (Cherepivska and Prihod, 2014; Bujdák, 2020; Dąbrowski et al., 2005). The impact of organic compounds on water pollution is mainly caused by heavy industrialization. Faced with this worrying situation, most scientific research is moving towards an innovative process of implementing environmentally friendly treatments. These organic pollutants are non-biodegradable or poorly biodegradable (Ait Ahsaine, 2018). Like most pollutants, phenol is harmful. It has been found in the wastewater of many industrial units, such as chemical, petrochemical, pharmaceutical, resins, coking, pesticides, and textile and paper industries(Krstić et al., 2011; Mobarak, 2019). Phenol has an unpleasant odor and taste and is toxic to aquatic organisms, plants, and humans at concentrations of 5 $\mu g{\cdot}L^{-1}$ (Dehmani et al., 2022; Dehmani and Lain, 2023). Long-term ingestion of phenol at concentrations between 10 and 240 mg/L can cause oral irritation, blurred vision, and diarrhea (Dehmani et al., 2022; Dehmani and Lain, 2023). Therefore, this pollutant often appears in rivers, seawater, industrial waste, urban wastewater, and even groundwater. Among all the methods of treatment of wastewater loaded with organic compounds, the adsorption of phenol on solid supports such as activated carbon, clay, and transition metal oxides allows their removal from water with a high removal rate without the addition of chemicals (Krstić et al., 2011; Mobarak, 2019; Dehmani et al., 2022; Dehmani and Lain, 2023; Bazrafshan et al., 2013; Malakootian et al., 2017; Malakootian et al., 2018; Babapour, 2022). Transition metal oxides have surface and textural properties that can play an important role in adsorbate binding. In addition, the crystalline nature of these solids makes it easier to study the mechanism of adsorption by computer tools (Daou et al., 2017; Sohrabi et al., 2021). One of these families of materials is cobalt oxide, which is a very important functional material, due to its electrical, structural, optical, and catalytic properties. The latter has been used in several areas, namely in the field of batteries, the field of electrochemical capacitors, optical materials, and the field of catalysis (Dehbi et al., 2019; Guan, 2021; Behnajady and Bimeghdar, 2014; Medina-Valtierra et al., 2009; Abbas et al., 2019).

Based on their structural and textural properties, many researchers have used cobalt oxide in the adsorption of various pollutants. R. F. Abbas and his collaborators have used this material for the removal of doxycycline hyclate (Abbas et al., 2019). The research team of Mostafa R. Abukhadra was interested in the adsorption of Congo red by Co3O4 (Abukhadra et al., 2019). The adsorption of ethylene carbonate has been studied and presented in the study of Fingerle et al. (2017). This research work mentions the important efficiency of Cobalt oxide in the removal of inorganic pollutants. Therefore, we thought about expanding the study of Cobalt oxide in the removal of organic compounds like phenol.

The objective of the present work on the one hand is to study the adsorption capacity of aqueous phenol on cobalt oxide prepared and characterized by physicochemical methods and on the other hand, a thorough study of the adsorption mechanism of phenol on cobalt oxide based on theoretical calculations made by DFT and advanced modeling of experimental data of the adsorption isotherm of phenol on cobalt oxide by advanced statistical physics models.

2. Experimental part

2.1. Preparation of the adsorbent

A mass (70 g) of dehydrated cobalt nitrate Co $(NO_3)_2$ $6H_2O$ was dissolved in one volume of distilled water. To this mixture was added dropwise (7 ml/min) a molar solution of NOH. The mixture obtained is filtered under a vacuum. The solid obtained is washed several times with hot distilled water and then dried overnight in an oven at 100 °C. Then calcined at 500° C for 3 h.

2.2. Characterization of the adsorbent

XRD: The X-ray diffraction (XRD) patterns were obtained using an X'PERT MPD-PRO wide-angle X-ray powder diffractometer supplied with a diffracted beam monochromator CuKα radiation (λ = 1.5406 Å). The voltage was 45 kV and therefore the intensity was 40 mA. The θ angle was scanned between 4° and 30°, and therefore the counting time was 2.0 s at each angle step (0.02°).

FTIR: The structural changes, which happened during the degradation of the samples studied, were collected within the Fourier Transform Infrared Spectrometer (FTIR) (Shimadzu, JASCO 4100). The samples were prepared in KBr discs in the usual way from alright dried mixtures of about 4 % (w/w). FTIR spectra were recorded by the buildup of a minimum of 64 scans with a resolution of 4 cm^{-1} per sample.

SEM: SEM images (SEM) were obtained by Brand EIF Quanta 200 apparatus equipped withenergydispersiveX-ray spectroscopy (EDX).

BET: N_2 adsorption measurements at T = − 196 °C were performed using Micromeritics ASAP 2010. The precise area and therefore the average pore diameter was determined in line with the quality BET and BJH (Barrett, Joyner, and Halenda) methods, respectively.

2.3. Point of zero charge

The determination of the zero charge point pH of cobalt oxide was performed according to a simple procedure indexed in the work of Dehmani (Dehmani et al., 2021).

2.4. Adsorption experiments

The phenol adsorption experiments are carried out according to the following procedure: at a constant temperature (T = 20, 40 and 60 °C) for a pH = 4 and with a stirring of 400 rpm for a period of adsorption between 0 and 180 min, a solution of phenol (20 ml) with a concentration that varies between 10 mg/l and 50 mg/l, is bound to a mass of 100 mg of Co_3O_4. At the end of the reaction, mixtures are filtered is analyzed by UV/Visible. This residual concentration was determined based on a UV spectrometer calibration curve/Visible at λ = 270 nm (Shimadzu UV-1240). The Eq. (1) is used to determine the amount adsorbed:

$$Q_{ads} = \frac{C_0 - C_e}{m_{adsorbant}} \times V_{sol}(mg/g) \quad (1)$$

Q is the adsorption capacity (mg/g), C_0 is the initial concentration of the phenol (mg/L), Ce is the residual concentration of the phenol (mg/L), m is the mass of adsorbent used (g) and V is the volume of the solution (L).

a. Adsorption kinetics

In this experiment, Lagergren's quasi-first-order kinetic equation, quasi-second-order kinetics equation, and intergranular diffusion equation were used to fit the dynamics.

Lagergren quasi-first order kinetic equation:

$$q_t = q_e(1 - e^{K_1 * t}) \quad (2)$$

Lagergren quasi-second-order kinetics equation:

$$q_t = \frac{K_2 * t * q_e^2}{1 + q_e * K_2 * t} \quad (3)$$

In these equations, qe is the adsorption capacity at balance (mg/g), qt is the adsorption capacity at any time (mg/g), and K_1 is the Lagergren first-order kinetics constant (min^{-1}), K_2 is the Lagergren second-order kinetics constant (g/min mg), and c is a constant related to the Boundary layer thickness (g/mg min).

b. Adsorption isotherms

Creating an adsorption isotherm for phenol on a solid requires the determination of the amount adsorbed as a function of the concentration in the equilibrium solution at a chosen temperature. The adsorption isotherm was fitted by the Freundlich model and the Langmuir model. The latter is the most quoted and used three-parameter model in the literature because it is applicable over a wide range of concentrations. It is an empirical equation developed by the Langmuir and Freundlich equation. It is widely used as a compromise between the Freundlich and Langmuir models, this model approximates the Freundlich model for high concentrations and the Langmuir equation for low concentrations. The nonlinear equations of these models:

Langmuir adsorption isotherm.

$$q_e = \frac{q_m * K_L * C_e}{1 + K_L * C_e} \quad (4)$$

Freundlich adsorption isotherm:

$$q_e = K_F * C_e^{1/n} \quad (5)$$

In these equations, Ce is the solution concentration at equilibrium (mg/L); qe is the adsorption capacity of the adsorbent for equilibrium (mg/g); qm is the theoretical saturated adsorption capacity of the adsorbent (mg/g) and K_L, K_F is the Langmuir, Freundlich constants respectively, and n relates to adsorption intensity.

2.5. Theoretical studies

a. Quantum chemical calculations

The Fukui indices were calculated using the DMol3 module embedded within the Material Studio (MS, version 7.0) and supported generalized gradient approximation (GGA) of Perdew–Burke Ernzerhof (PBE) and "double numeric plus polarization" (DNP, setting to 4.4) (Chugh et al., 2020). All DFT calculations used Dmol3 default convergence criteria for geometry optimization, and the quality is "fine". The Fukui functions are obtained through the finite difference approximation during a vacuum and water using Hirshfeld population analysis (HPA).

b. Molecular dynamics simulations

Molecular dynamics (MD) calculations during this study were allotted via a simulation box together with periodic boundary conditions employing a materials studio package. Co3O4 was cleaved to the (1 1 1) plane, which is the most stable form Yu et al. (2013). The Co3O4 (1 1 1) surface was made via a simulation box (21.04 × 21.04 × 29.35 Å3), and a vacuum region, which is placed above the highest surface, is ready as 13 A° to eliminate unwanted interactions between adjacent slabs. Moreover, 100 water molecules were used as a model for the solvent effect on the adsorption capacity of phenol on the Co3O4 (1 1 1) surface. MD simulations were disbursed employing the COMPASS physical phenomenon (Sun, 1998). Within the Forcite module, the NVT ensemble with the velocity-Verlet integration algorithm and a time step of 1.0 fs, at temperature 298 K controlled by Nosé-Hoover thermostat was used. Electrostatic interactions were treated by utilizing the Ewald method, and also the atom-based cutoff summation method was applied for van der Waals. After the energy minimization, each simulation was performed for 500 ps within the NVT ensemble to achieve the equilibration state. The Phenol-Co3O4 (1 1 1) interaction energies in a very vacuum and water were calculated by Eq. (6) and Eq. (7), respectively (Barbouchi et al., 2020):

$$E_{interaction} = E_{total} - (E_{surface+solution} + E_{phenol}) \quad (6)$$

$$E_{binding} = -E_{interaction} \quad (7)$$

where E_{total} denotes the all-system energy, $E_{surface+H2O}$ and $E_{surface}$ designate, respectively, the Co_3O_4 (1 1 1) energy alone and including water molecules, E_{Phenol} implies the energy of the phenol molecule.

3. Results and discussion

3.1. Solid characterization

a. XRD

X-ray diffraction patterns of pure cobalt oxide nanoparticles are shown in Fig. 1. XRD models show very intensely, prominent, and sharp diffraction peaks demonstrating the

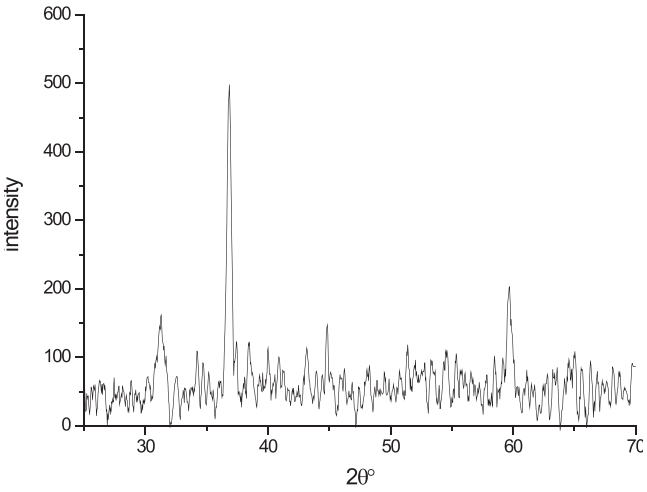

Fig. 1 XRD of cobalt oxide.

crystalline nature of the synthesized Co3 O4 nanoparticles. Net diffraction peaks of pure Co3O4 nanoparticles are observed at 2θ values of 31.6°, 37.3°, 44.7°, 59.4° and 65.2° would be attributed to the crystalline planes (220), (311), (400), (511) and (440) respectively. These peaks correspond to cubic Co3O4 structured in line with the JCPDS card number (14–0673) (Manjula et al., 2021; Vázquez-Vargas, 2020; Osakoo, 2020; Mayakannan et al., 2018; Yasin et al., 2007).

From the Scherrer relation (N) we can determine the particle diameter of the solid. The average grain size (d) of the films was evaluated.

$$d = \frac{0.94 * \lambda}{\cos(\Theta) * \beta}$$

λ, θ and β are the wavelength of X-rays (1.54 (A), the corner of Bragg diffraction and the width of stripe to half the maximum of (311) around 37.3°. The average size of the grain of our samples is 31.23 nm.

b. **FTIR**

The Fig. 2 shows the infrared Fourier transform spectra for the prepared solid. All the bands and their attributions are grouped in Table 1. It may be noted that the bands of the infrared spectra referring to the solids prepared within the presence of ammonia are more intense than those of the solids prepared within the presence of hydroxide. In addition, the bands at 2917, 2851, and 1573 cm-1 could be attributed to impurities that come from the air or to the humidity of KBr (Manjula et al., 2021).

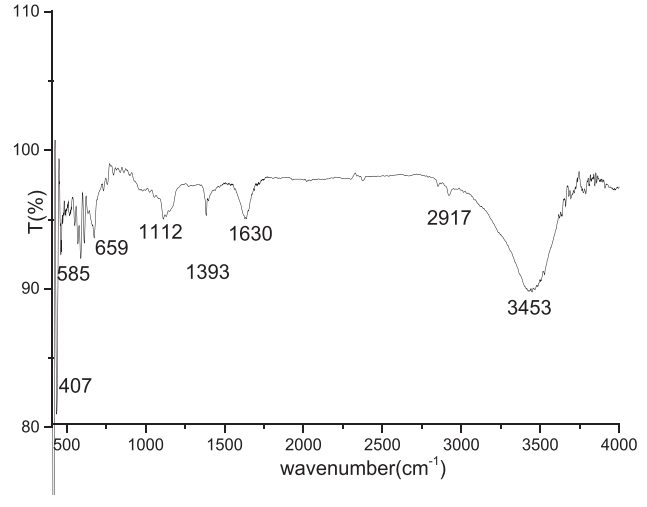

Fig. 2 Infrared spectroscopy for the Cobalt oxide.

c. **SEM**

Fig. 3 shows the scanning microscopy image of cobalt oxide prepared by the precipitation method with the precipitating agent sodium hydroxide; the image shows an identical agglomerated morphology. The diffractogram shows the existence of the essential elements of our oxide with well-defined percentages of Co (51.97 %) and O (48.03 %).

d. **BET**

The isotherm of adsorption/desorption of nitrogen on cobalt oxide prepared shows that we have an isotherm of IV (Fig. 4) with an H_3 type hysteresis loop which characterizes the mesoporous materials. This solid has a surface area of the order of 12 m^2/g.

e. **Point of zero charge**

The pH of the zero charge point corresponds to the pH value that the online charge on the surface of the adsorbents is zero. This parameter is extremely important in adsorption phenomena. From Fig. 5 we discover that the pHpcn = 8.28. The dominant charge on the solid surface is negative within the case of pH > 8.28 and positive within the other case.

3.2. Adsorption of phenol on cobalt oxide

a. **Effect of contact time**

The study of the influence of the contact time on the adsorption of phenol by the transition metal oxides may be a significant step because it allows determining the time necessary to achieve equilibrium. The results obtained are grouped in Fig. 6, which illustrates the evolution of the number of phenol adsorbed on Co3O4 as a function of your time. The analysis of those curves shows that the adsorption rate of phenol on cobalt oxide evolves rapidly during the primary minutes of contact and so stabilizes as saturation is approached. The fast adsorption kinetics, observed at the start of the method, is interpreted by the fact that at the start of the adsorption

Table 1 Bands and types of vibration for the two solid.

Bands (cm^{-1})	Types of vibration
3453	**H—O—H**
1630	**H—O—H**
1393	**CO_2**
1112	**H—O—H**
659	**Co—O**
609	**Co—O**
585	**Co—O**
470	**Co—O**

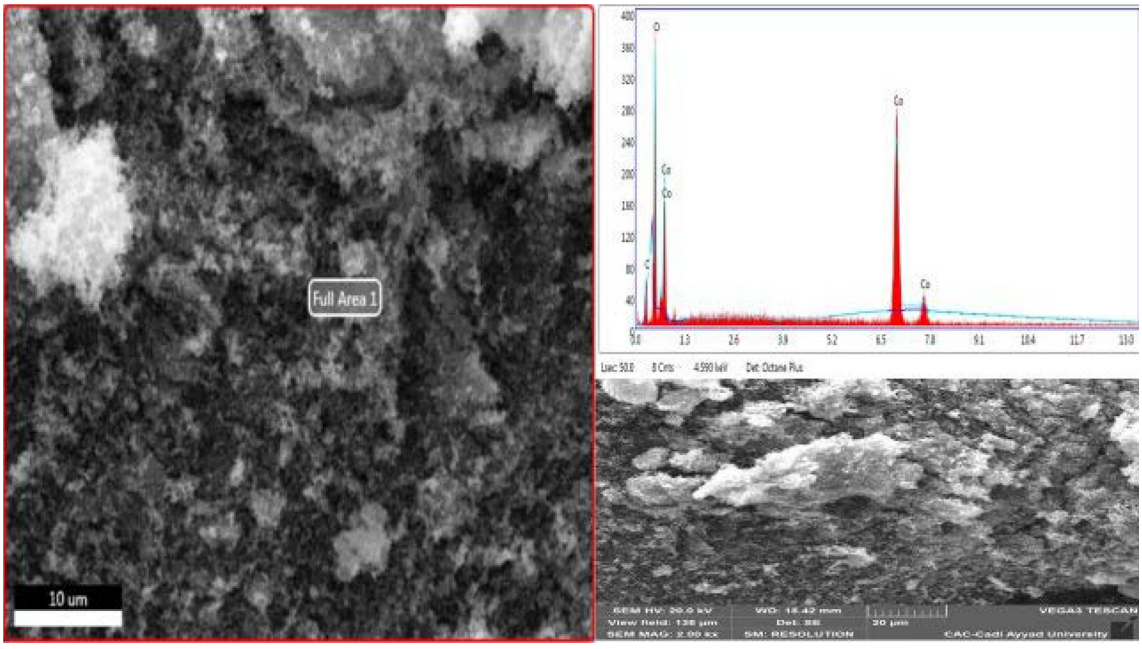

Fig. 3 SEM images of cobalt oxide.

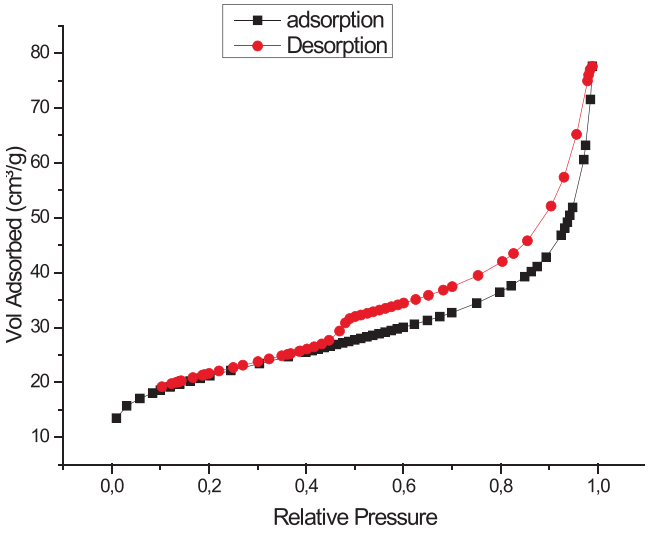

Fig. 4 Nitrogen adsorption and desorption isotherms as a function of relative pressure of cobalt oxide.

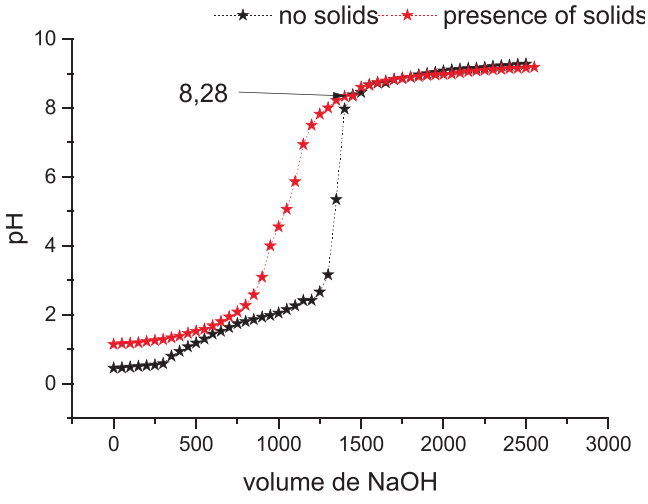

Fig. 5 Point of Zero Charge.

the quantity of active sites available on the surface of the cobalt oxide is very important (Lütke et al., Oct. 2019; Feng, Apr. 2020). After it slows, the remaining vacant sites become difficult to access because of the existence of repulsive forces between the phenol molecules adsorbed by the cobalt oxide and people in the solution. Stabilization of the adsorbed amount is observed beyond 60 min of duration. To make sure that equilibrium is reached in which there is no desorption of the adsorbed molecules, we fixed the solid-solution contact time for the remainder of our experiments at 120 min. The results of the contact time effect on phenol adsorption show that the phenomenon is fast and the reaching of saturation does not exceed 20 min, which is explained by the great variety of interactions between the phenol molecules and the prepared solid particles.

b. **Effect of pH**

The study of the influence of pH on the adsorption of phenol on cobalt oxide was applied using solutions of phenol (20 mg/l) in grips with the adsorbent at the concentration of the oxide and for pH values varying between 1.5 and 5. The results obtained are presented in Fig. 7. The figure shows us, that the adsorption efficiency of phenol increases with the rise of the initial pH of the organic solution. The very best value of this percentage is obtained for a pH = 4, this value is about 98 %. At low pH, thanks to the high density of the electric charge because of the protons of the cobalt oxide, the electrostatic repulsion is going to be higher during the adsorption

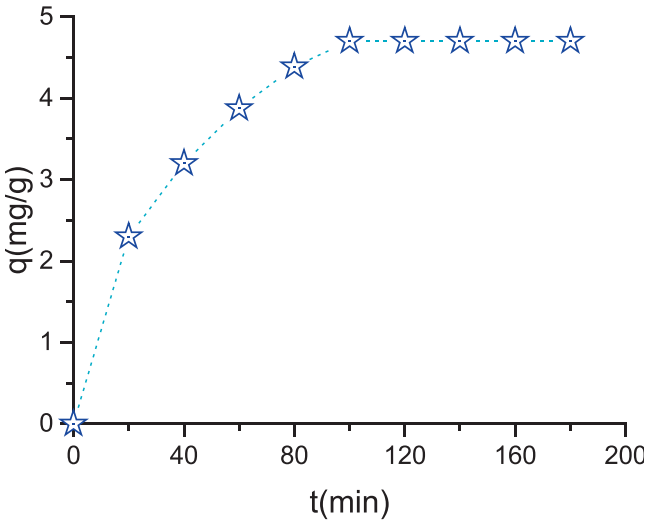

Fig. 6 Effect of contact time on adsorption (T = 30 °C; pH = 4; m = 100 mg; C = 30 mg/L).

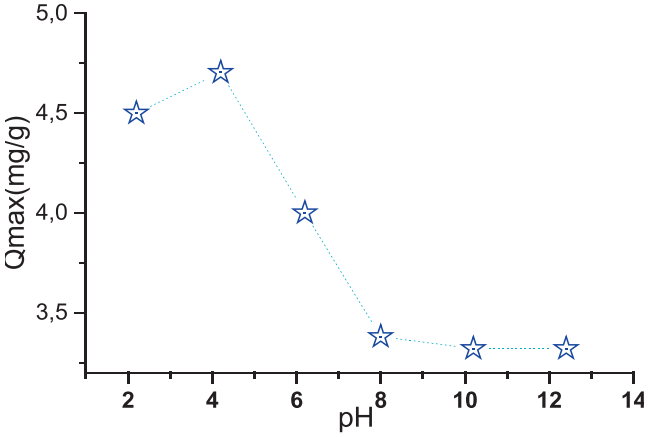

Fig. 7 Effect of pH on adsorption (T = 30 °C; t = 180 min; m = 100 mg; C = 30 mg/L).

process leading to a decrease in the extraction efficiency. Increasing the pH causes the electrostatic repulsion to decrease; this is often thanks to the reduction of the electric charge density on the active sites of the adsorbent increasing the adsorption efficiency of the phenol ions. At higher pH values, OH ions compete with phenol ions to occupy the active sites on the surface of the adsorbent ions to occupy the active sites on the adsorbent surface (Taylor et al., 2015; Li, 2012).

c. Effect of temperature on adsorption

The temperature is an important factor that conditions the behavior of an adsorbate towards an adsorbent. Moreover, the solubility of a salt is a function of the temperature of the medium. From Fig. 8 we can see that the adsorption efficiency of phenol decreases when the temperature decreases, which suggests that we are in the presence of an endothermic adsorption phenomenon. A temperature higher than 50 °C has the effect of destabilizing the adsorption forces involved, so it is the optimal value to promote the adsorption of phenol and this means

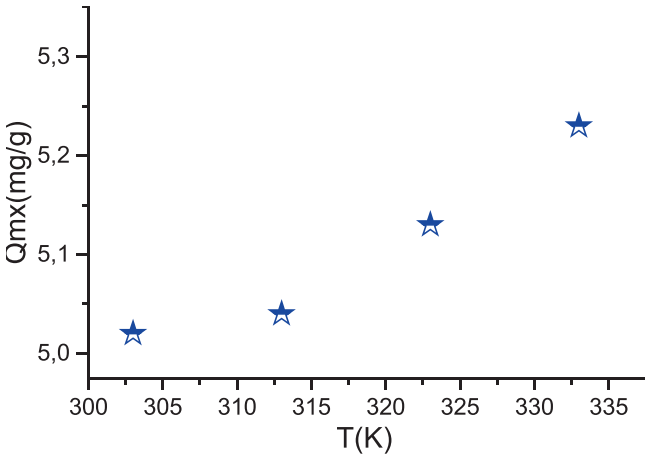

Fig. 8 Effect of Temperature on adsorption (t = 180 min; pH = 4; m = 100 mg; C = 30 mg/L).

that the adsorption process could be endothermic and would lead to chemisorption.

d. Kinetic

The experimental kinetic data were fitted to the models represented by Eqs. (2) and (3). The results are presented in Fig. 9. The parameters of the pseudo-first-order and pseudo-second-order diffusion models were obtained by using linear plots and determining the slopes and intercepts. The pseudo-first-order equations don't adequately represent the experimental data. This can be per the relatively low value of the parametric statistic $R^2 < 0.59$, and also the inconsistency between the fitted and experimental values (Rong et al., 2015; Dehmani et al., 2021; Aksu and Akpinar, 2000). A pseudo-second-order model fully describes the kinetic behavior of the removal of this contaminant on cobalt oxide ($R^2 > 0.99$). This suggests that the removal process is especially driven by chemisorption and also depends on the physicochemical interaction between cobalt oxide and phenol (Aksu and Akpinar, 2000). According to this result, the adsorption is of chemisorption type, with the forma-

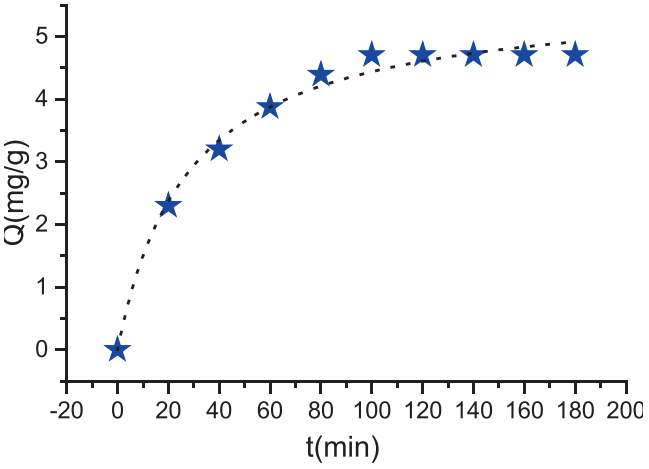

Fig. 9 kinetic data modelling (T = 30 °C; pH = 4; m = 100 mg; C = 30 mg/L).

tion of valence bonds between the surface functions of the oxide and the phenol molecules.

e. **Adsorption isotherm**

The mechanism of interaction between phenol and cobalt oxide is often elucidated by determining the equilibrium adsorption isotherms and kinetics of the systems. The model parameters were calculated by minimizing Eq. (5) and validated using Eq. (6). The results obtained by fitting the various adsorption isotherms to the experimental data are presented in Fig. 10, while the corresponding constants are shown in Table 1 for the adsorption of phenol on cobalt oxide, Fig. 5 (Gimbert et al., 2008; Crini et al., 2007; Xu, 2022; Ba Mohammed, 2021). Langmuir isotherms best describe the adsorption of phenol on cobalt oxide with (R2 = 0.9975) with a smaller value of MPSD (MPSD = 9.3608). The Freundlich model gave very cheap

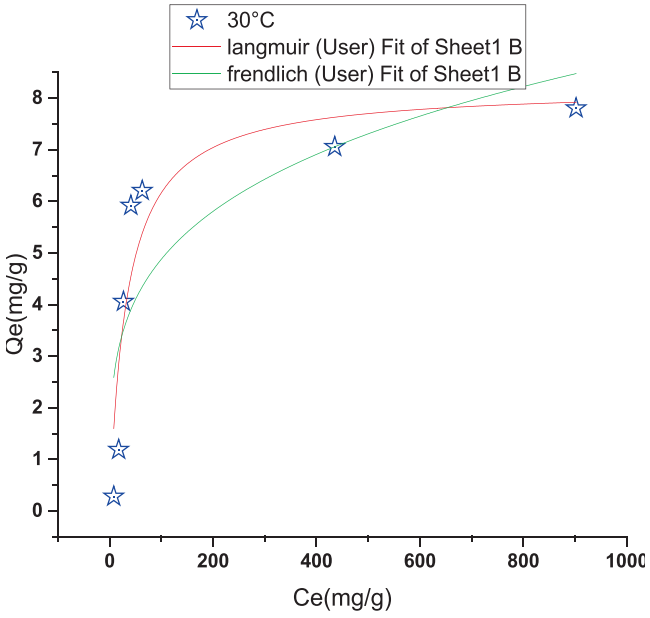

Fig. 10 modeling of the adsorption isotherm (T = 30 °C; pH = 4; m = 100 mg; t = 180 min).

parametric statistic values (R2 = 0.9774), suggesting a poor fit and a non-significant representation of the experimental data. The particular adsorption results improved significantly from our initial results from an adsorption capacity of 2 mg/g to five mg/g for phenol, this can be mainly attributed to the optimized pH conditions. Although the results show a decent fit and high percentage removal(94 %), the adsorption capacity of cobalt oxide remains significantly low compared to other adsorbents like NaY zeolite (Dehmani et al., 2021)(also as 25 mg/g for titanium/graphene composite catalysts (Jiang et al., 2002), clay materials (48 mg/g for modified clay) (Awad, 2019), a biochar-based iron oxide composite bee (39 mg/g for phenol) (Dong, 2021), and a dual magnetic network nanocomposite hydrogel (66 mg/g (Nakhjiri et al., Apr. 2021). However, cobalt oxide has comparable adsorption capacity to other adsorbents like Na-bentonite (3.7 mg/g for phenol (Asnaoui et al., 2020), nickel, iron, and zinc oxides (10 mg/g for phenol (Dehmani et al., 2021; Dehmani and Abouarnadasse, 2020; Dehmani et al., May 2020). The adsorption capacities within the present study were over the 5 adsorbents reported by Md. (Ahmaruzzaman, 2008), namely FA wood (5 mg/g), aluminum pillar bentonite (1.8 mg/g), modified clarion clay (1.24 mg/g), bentonite (1.7 mg/g) and thermal bentonite (1.30 mg/g) (Ahmaruzzaman, 2008).

3.3. Quantum chemical calculations

To determine the sites accountable for the interactions between cobalt oxide and therefore the phenol molecule. Local electronic parameters like Fukui functions for the phenol molecule in an exceedingly vacuum and water are calculated. The Fukui indices f- allows us to differentiate the various functional groups chargeable for electrophilic attacks, while the nucleophilic attack is distinguished by Fukui indices f+.

The results of the Fukui indices obtained in Table 2 for phenol in a very vacuum and water show that the high values of f- are located on the oxygen atoms O (1), C (2), C (3), and C (7). So it can easily give electrons, also the high value of f+ which is localized on atoms C(3), C (4), C (5), and C(6) indicates that this site can easily accept electrons (Berrissoul et al., 2020). Therefore, explain the electron density distribution of phenol molecule as an adsorbed compound on the

Table 2 The Fukui indices of electrophilic and nucleophilic behaviors of phenol compound.

	Fukui indices in vacuum		**Fukui indices in water**	
	Electrophilic Attack (f^-)	**Nucleophilic Attack (f^+)**	**Electrophilic Attack (f^-)**	**Nucleophilic Attack (f^+)**
O (1)	**0.132**	0.052	**0.137**	0.041
C (2)	**0.095**	0.056	**0.105**	0.061
C (3)	**0.096**	**0.123**	**0.102**	**0.132**
C (4)	0.091	**0.124**	0.101	**0.134**
C (5)	0.074	**0.130**	0.076	**0.138**
C (6)	0.076	**0.128**	0.076	**0.136**
C (7)	**0.142**	0.067	**0.148**	0.072
H (8)	0.049	0.060	0.044	0.057
H (9)	0.047	0.060	0.042	0.056
H (10)	0.046	0.062	0.037	0.058
H (11)	0.046	0.062	0.037	0.058
H (12)	0.058	0.044	0.053	0.037
H (13)	0.049	0.030	0.044	0.020

metal oxide surface. The tabulated Fukui functions values and therefore the extracted electronic density surface results (depicted in Fig. 11) manifest that the electrophilic/nucleophilic type attacks of phenol molecule in vacuum have an identical appearance to those in water.

3.4. Molecular dynamics simulations

In this section, we used MD simulations to explore the mechanism of adsorption of the phenol molecule on the cobalt oxide (Co3O4) surface. Co3O4 is in a very cubic spinel structure, with a space group of Fd3m. The relaxed structure of the cubic Co3O4 is shown in Fig. 12a. The structure of the Co3O4 spinel consists of CoO6 octahedrons (Fig. 12b) and CoO4 tetrahedrons (Fig. 12. c). (Xu et al., 2009; Yu et al., 2013). Therefore, simulations were disbursed in both vacuum and therefore the presence of water molecules (solvent), in a trial to mimic the effect of the solvent in the maximum amount possible. Fig. 13 shows that phenol molecules in both vacuum and water phases are found to lie parallel to the cobalt oxide surface, with more close contact with the cobalt oxide surface within the presence of water. The phenol molecule adsorbed on

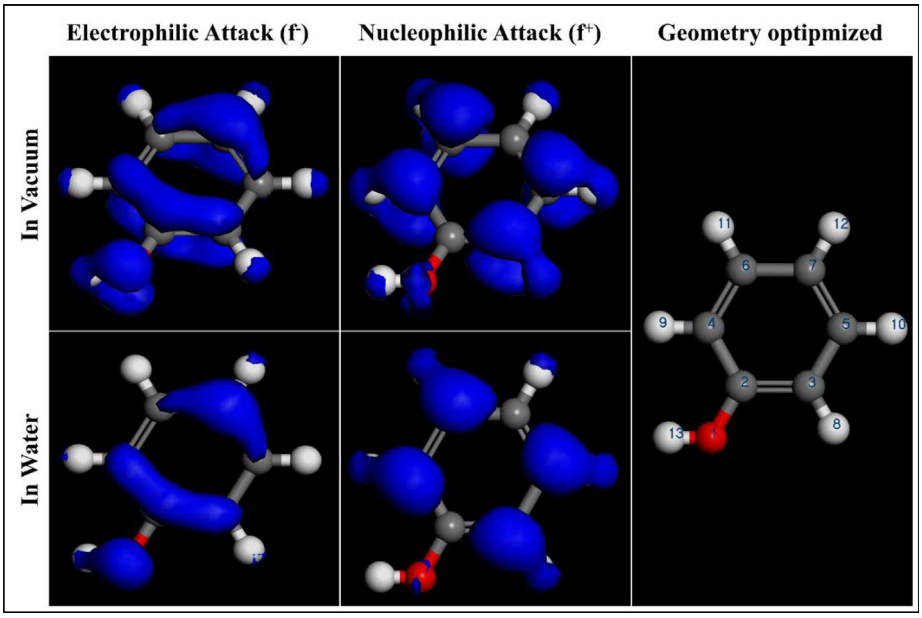

Fig. 11 Fukui functions for phenol molecule calculated by DFT (Dmol3). Geometry optimized structure, nucleophilic and electrophilic Fukui functions.

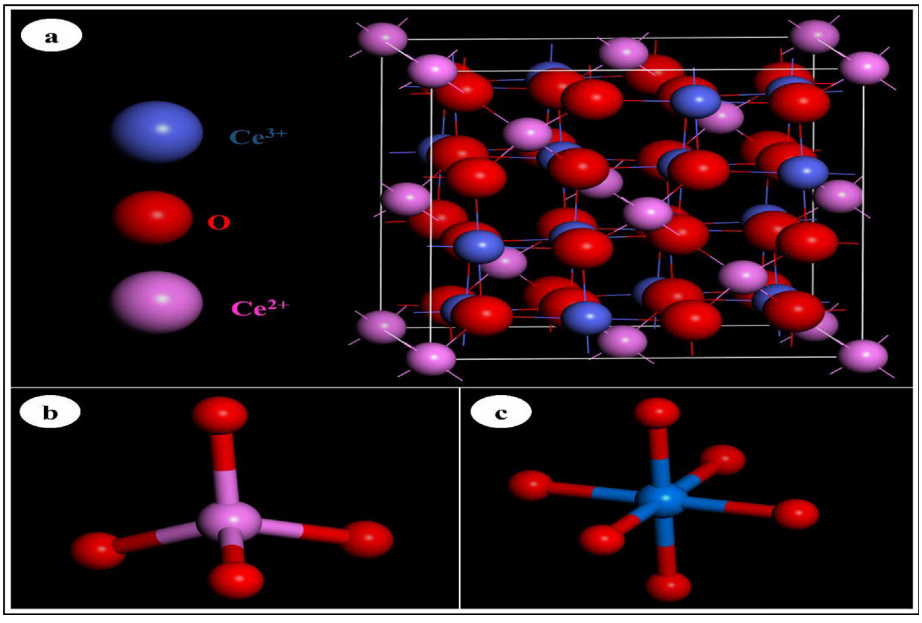

Fig. 12 Schematic views of the relaxed atomic structure of the Co_3O_4 compound (a), tetrahedron CoO_4 (b) and octahedron CoO_6 (c).

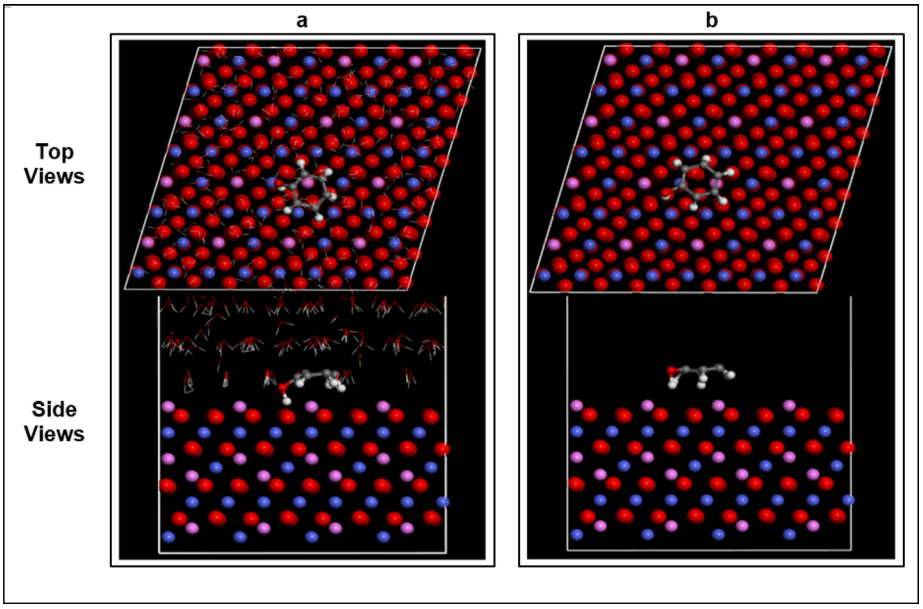

Fig. 13 Configurations of phenol molecules adsorption on Co_3O_4 (1 1 1) surface obtained by MD simulations, (a) In the presence of water molecules and (b) In vacuum.

Table 3 Interaction and binding energies obtained from MD simulations for adsorption of phenol on Co_3O_4 (1 1 1) surface.

Simulations models	$E_{interaction}$ (KJ/mol)	$E_{binding}$ (KJ/mol)
Co_3O_4 (1 1 1) + Phenol + 100 H_2O	**−236.936**	**236.936**
Co_3O_4 (1 1 1) + Phenol	**−197.040**	**197.040**

the cobalt oxide surface within the presence of water exhibits an energy of 2369.36 kJ/mol, which is larger than that during a vacuum of 1970.40 kJ/mol (see Table 3).

4. Conclusion

The object of this work is the preparation and characterization of cobalt oxide yet as its application to the adsorption of phenol within the aqueous medium. We could obtain an oxide of porous texture and structural properties as confirmed therewith in the literature. The adsorption capacity of phenol on the solid used depends on the pH and temperature. We could show that at acidic pH the adsorption of phenol is healthier because of the dominant dispersive forces while at basic pH the dissociation of phenol molecules into phenolates disadvantages the adsorption. Additionally, to probe the adsorption action of the phenolic emulsion on the cobalt oxide face, theoretical simulations grounded on MD (molecular dynamics) and DFT (viscosity functional proposition) were performed. DFT results verified the ascendance of chemisorption while MD simulations indicated enhanced commerce of Co3O4 with phenol within the presence of detergent because of water-bridged H- bonds. The results obtained show that the solid prepared has an adsorption capacity of 94 %; this material may be utilized in wastewater treatment plants.

Declaration of Competing Interest

The authors declare that they have no known competing financial interests or personal relationships that could have appeared to influence the work reported in this paper.

Acknowledgment

The authors would like to thank the Deanship of Scientific Research at Umm Al- Qura University. 22UQU4331100DSR01.

References

Dąbrowski, A., Podkościelny, P., Hubicki, Z., Barczak, M., 2005. Adsorption of phenolic compounds by activated carbon - A critical review. Chemosphere 58 (8), 1049–1070. https://doi.org/10.1016/j.chemosphere.2004.09.067.

Abbas, R.F., Hami, H.K., Mahdi, N.I., 2019. Removal of doxycycline hyclate by adsorption onto cobalt oxide at three different temperatures: isotherm, thermodynamic and error analysis. Int. J. Environ. Sci. Technol. 16 (10), 5439–5446. https://doi.org/10.1007/s13762-018-2079-y.

Abukhadra, M.R., Adlii, A., Bakry, B.M., 2019. Green fabrication of bentonite/chitosan@cobalt oxide composite (BE/CH@Co) of enhanced adsorption and advanced oxidation removal of Congo red dye and Cr (VI) from water. Int. J. Biol. Macromol. 126 (Vi), 402–413. https://doi.org/10.1016/j.ijbiomac.2018.12.225.

Ahmaruzzaman, M., 2008. Adsorption of phenolic compounds on low-cost adsorbents: A review. Adv. Colloid Interface Sci. https://doi.org/10.1016/j.cis.2008.07.002.

Ait Ahsaine, H. et al, 2018. Cationic dyes adsorption onto high surface area 'almond shell' activated carbon: Kinetics, equilibrium isotherms and surface statistical modeling. Mater. Today Chem. 8, 121–132. https://doi.org/10.1016/j.mtchem.2018.03.004.

Aksu, Z., Akpinar, D., 2000. Modelling of simultaneous biosorption of phenol and nickel(II) onto dried aerobic activated sludge. Sep. Purif. Technol. https://doi.org/10.1016/S1383-5866(00)00194-5.

Asnaoui, H., Dehmani, Y., Khalis, M., Hachem, E.K., 2020. Adsorption of phenol from aqueous solutions by Na–bentonite: kinetic, equilibrium and thermodynamic studies. Int. J. Environ. Anal. Chem. 00 (00), 1–15. https://doi.org/10.1080/03067319.2020.1763328.

Awad, A.M. et al, 2019. Adsorption of organic pollutants by natural and modified clays: A comprehensive review. Sep. Purif. Technol.

228 (January), 115719. https://doi.org/10.1016/j.seppur.2019.115719.
Ba Mohammed, B. et al, 2019. Adsorptive removal of phenol using faujasite-type Y zeolite: Adsorption isotherms, kinetics and grand canonical Monte Carlo simulation studies. J. Mol. Liq., 111997 https://doi.org/10.1016/j.molliq.2019.111997.
Ba Mohammed, B. et al, 2021. Enhanced removal efficiency of NaY zeolite toward phenol from aqueous solution by modification with nickel (Ni-NaY). J. Saudi Chem. Soc. 25 (4), 101224. https://doi.org/10.1016/j.jscs.2021.101224.
Babapour, M. et al, 2022. Adsorption of Cr(VI) from aqueous solution using mesoporous metal-organic framework-5 functionalized with the amino acids: Characterization, optimization, linear and non-linear kinetic models. J. Mol. Liq. 345, 117835. https://doi.org/10.1016/j.molliq.2021.117835.
Barbouchi, M., Benzidia, B., Aouidate, A., Ghaleb, A., El Idrissi, M., Choukrad, M., 2020. Theoretical modeling and experimental studies of Terebinth extracts as green corrosion inhibitor for iron in 3 % NaCl medium. J. King Saud Univ. - Sci. 32, 2995–3004. https://doi.org/10.1016/j.jksus.2020.08.004.
Bazrafshan, E., Kord Mostafapour, F., Jafari Mansourian, H., 2013. Phenolic Compounds: Health Effects and Its Removal From Aqueous Environments by Low Cost Adsorbents. Heal. Scope 2 (2), 65–66. https://doi.org/10.17795/jhealthscope-12993.
Behnajady, M.A., Bimeghdar, S., 2014. Synthesis of mesoporous NiO nanoparticles and their application in the adsorption of Cr(VI). Chem. Eng. J. 239, 105–113. https://doi.org/10.1016/j.cej.2013.10.102.
Berrissoul, A., Ouarhach, A., Benhiba, F., Romane, A., Zarrouk, A., Guenbour, A., Dikici, B., Dafali, A., 2020. Evaluation of Lavandula mairei extract as green inhibitor for mild steel corrosion in 1 M HCl solution. Experimental and theoretical approach. J. Mol. Liq. 313, 113493. https://doi.org/10.1016/j.molliq.2020.113493.
Bujdák, J., 2020. Applied Clay Science Adsorption kinetics models in clay systems. The critical analysis of pseudo- second order mechanism. Appl. Clay Sci. 191 (February), 105630. https://doi.org/10.1016/j.clay.2020.105630.
Cherepivska, M.K., Prihod, R.V., 2014. "Sol-Gel Synthesized Semiconductor Oxides in Photocatalytic Degradation of. Phenol" 3, 2014.
Chugh, B., Singh, A.K., Chaouiki, A., Salghi, R., Thakur, S., Pani, B., 2020. A comprehensive study about anti-corrosion behaviour of pyrazine carbohydrazide: Gravimetric, electrochemical, surface and theoretical study. J. Mol. Liq. 299, 112160. https://doi.org/10.1016/j.molliq.2019.112160.
Crini, G., Peindy, H.N., Gimbert, F., Robert, C., 2007. Removal of C. I. Basic Green 4 (Malachite Green) from aqueous solutions by adsorption using cyclodextrin-based adsorbent: Kinetic and equilibrium studies. Sep. Purif. Technol. https://doi.org/10.1016/j.seppur.2006.06.018.
Daou, I., Zegaoui, O., Elghazouani, A., 2017. Physicochemical and photocatalytic properties of the ZnO particles synthesized by two different methods using three different precursors. Comptes Rendus Chim. 20 (1), 47–54. https://doi.org/10.1016/j.crci.2016.04.003.
Dehbi, A., Dehmani, Y., Omari, H., Lammini, A., Elazhari, K., Abdallaoui, A., 2019. Hematite Iron Oxide Nanoparticles (α-Fe2O3): Synthesis and Modelling Adsorption of Malachite Green. J. Environ. Chem. Eng. 8 (1), 103394. https://doi.org/10.1016/j.jece.2019.103394.
Dehmani, Y., Abouarnadasse, S., 2020. Study of the adsorbent properties of nickel oxide for phenol depollution. Arab. J. Chem. 13 (5), 5312–5325. https://doi.org/10.1016/j.arabjc.2020.03.010.
Dehmani, Y., Alrashdi, A.A., Lgaz, H., Lamhasni, T., Abouarnadasse, S., Chung, I.M., May 2020. Removal of phenol from aqueous solution by adsorption onto hematite (α-Fe2O3): Mechanism exploration from both experimental and theoretical studies. Arab. J. Chem. 13 (5), 5474–5486. https://doi.org/10.1016/j.arabjc.2020.03.026.
Dehmani, Y., Dridi, D., Lamhasni, T., Abouarnadasse, S., Chtourou, R., Lima, E.C., 2022. Review of phenol adsorption on transition metal oxides and other adsorbents. J. Water Process Eng. 49 (March). https://doi.org/10.1016/j.jwpe.2022.102965.
Dehmani, Y., Lain, J., 2023. Unravelling the adsorption mechanism of phenol on zinc oxide at various coverages via statistical physics, artificial neural network modeling and ab initio molecular dynamics. Chem. Eng. J. 452 (September), 2022. https://doi.org/10.1016/j.cej.2022.139171.
Dehmani, Y., Lgaz, H., Alrashdi, A.A., Lamhasni, T., Abouarnadasse, S., Chung, I.M., 2021. Phenol adsorption mechanism on the zinc oxide surface: Experimental, cluster DFT calculations, and molecular dynamics simulations. J. Mol. Liq. 324, 114993. https://doi.org/10.1016/j.molliq.2020.114993.
Dehmani, Y., El Khalki, O., Mezougane, H., Abouarnadasse, S., 2021. Comparative study on adsorption of cationic dyes and phenol by natural clays. Chem. Data Collect. 33, 100674. https://doi.org/10.1016/j.cdc.2021.100674.
Dong, F.X. et al, 2021. Simultaneous adsorption of Cr(VI) and phenol by biochar-based iron oxide composites in water: Performance, kinetics and mechanism. J. Hazard. Mater. https://doi.org/10.1016/j.jhazmat.2021.125930.
Feng, D. et al, Apr. 2020. Functionalized construction of biochar with hierarchical pore structures and surface O-/N-containing groups for phenol adsorption. Chem. Eng. J. 410, 127707. https://doi.org/10.1016/j.cej.2020.127707.
Fingerle, M., Späth, T., Schulz, N., Hausbrand, R., 2017. Adsorption of ethylene carbonate on lithium cobalt oxide thin films: A synchrotron-based spectroscopic study of the surface chemistry. Chem. Phys. 498–499, 19–24. https://doi.org/10.1016/j.chemphys.2017.09.004.
Gimbert, F., Morin-Crini, N., Renault, F., Badot, P.M., Crini, G., 2008. Adsorption isotherm models for dye removal by cationized starch-based material in a single component system: Error analysis. J. Hazard. Mater. https://doi.org/10.1016/j.jhazmat.2007.12.072.
Guan, Y. et al, 2021. Catalytic combustion of volatile organic compounds (VOCs) over structured Co3O4 nano-flowers on silicalite-1/SiC foam catalysts. Micropor. Mesopor. Mater. 323 (April), 111173. https://doi.org/10.1016/j.micromeso.2021.111173.
Jiang, J.Q., Cooper, C., Ouki, S., 2002. Comparison of modified montmorillonite adsorbents Part I: Preparation, characterization and phenol adsorption. Chemosphere 47 (7), 711–716. https://doi.org/10.1016/S0045-6535(02)00011-5.
Krstić, J., Mojović, Z., Rabi, A.A., Lončarević, D., Vukelić, N., Jovanović, D., 2011. Adsorption of methylene blue from aqueous solution onto bentonite. Environ. Earth Sci., 1097–1106 https://doi.org/10.1007/978-3-540-95991-5-103.
Li, Y. et al, 2012. Equilibrium, kinetic and thermodynamic studies on the adsorption of phenol onto graphene. Mater. Res. Bull. 47 (8), 1898–1904. https://doi.org/10.1016/j.materresbull.2012.04.021.
Lütke, S.F., Igansi, A.V., Pegoraro, L., Dotto, G.L., Pinto, L.A.A., Cadaval, T.R.S., Oct. 2019. Preparation of activated carbon from black wattle bark waste and its application for phenol adsorption. J. Environ. Chem. Eng. 7 (5), 103396. https://doi.org/10.1016/j.jece.2019.103396.
Malakootian, M., Mansoorian, H.J., Alizadeh, M., Baghbanian, A., 2017. Phenol removal from aqueous solution by adsorption process: Study of the nanoparticles performance prepared from aloe vera and mesquite (prosopis) leaves. Sci. Iran. 24 (6), 3041–3052. https://doi.org/10.24200/sci.2017.4524.
Malakootian, M., Mahvi, A.H., Mansoorian, H.J., Khanjani, N., 2018. Agrowaste based ecofriendly bio-adsorbent for the removal of phenol: Adsorption and kinetic study by acacia tortilis pod shell. Chiang Mai J. Sci. 45 (1), 355–368.
Manjula, N., Vinothkumar, V., Chen, S.M., 2021. Synthesis and characterization of iron-cobalt oxide/polypyrrole nanocomposite: An electrochemical sensing platform of anti-prostate cancer drug flutamide in human urine and serum samples. Colloids Surfaces A

Physicochem. Eng. Asp. 628 (July), 127367. https://doi.org/10.1016/j.colsurfa.2021.127367.

Mayakannan, M., Gopinath, S., Vetrivel, S., 2018. Synthesis and characterization of antibacterial activities nickel doped cobalt oxide nano particles. Mater. Chem. Phys. 242 (October). https://doi.org/10.1016/j.matchemphys.2019.122282.

Medina-Valtierra, J., Frausto-Reyes, C., Camarillo-Martínez, G., Ramírez-Ortiz, J.A., 2009. Complete oxidation of isopropanol over Cu4O3 (paramelaconite) coating deposited on fiberglass by CVD. Appl. Catal. A Gen. 356 (1), 36–42. https://doi.org/10.1016/j.apcata.2008.12.014.

Mobarak, M. et al, 2019. Statistical physics modeling and interpretation of methyl orange adsorption on high–order mesoporous composite of MCM–48 silica with treated rice husk. J. Mol. Liq. 285, 678–687. https://doi.org/10.1016/j.molliq.2019.04.116.

Nakhjiri, M.T., Bagheri Marandi, G., Kurdtabar, M., 2021. Preparation of magnetic double network nanocomposite hydrogel for adsorption of phenol and p-nitrophenol from aqueous solution. J. Environ. Chem. Eng. 9 (2), 105039. https://doi.org/10.1016/j.jece.2021.105039.

Osakoo, N. et al, 2020. Development and characterization of silica supported cobalt oxides for ethanol oxidation using different preparation methods. Radiat. Phys. Chem. 171 (October), 108718. https://doi.org/10.1016/j.radphyschem.2020.108718.

Rong, X., Qiu, F., Zhang, C., Fu, L., Wang, Y., Yang, D., 2015. Adsorption-photodegradation synergetic removal of methylene blue from aqueous solution by NiO/graphene oxide nanocomposite. Powder Technol. 275, 322–328. https://doi.org/10.1016/j.powtec.2015.01.079.

Sohrabi, N., Mohammadi, R., Ghassemzadeh, H.R., Heris, S.S.S., 2021. Equilibrium, kinetic and thermodynamic study of diazinon adsorption from water by clay/GO/Fe3O4: Modeling and optimization based on response surface methodology and artificial neural network. J. Mol. Liq. 328, 115384. https://doi.org/10.1016/j.molliq.2021.115384.

Sun, H., 1998. COMPASS: An ab Initio Force-Field Optimized for Condensed-Phase ApplicationsOverview with Details on Alkane and Benzene Compounds. J. Phys. Chem. B. https://doi.org/10.1021/jp980939v.

Taylor, P., Asmaly, H.A., Abussaud, B., Saleh, T.A., Laoui, T., 2015. Desalination and Water Treatment Adsorption of phenol on aluminum oxide impregnated fly ash. Desalinat. Water Treatment (February), 37–41. https://doi.org/10.1080/19443994.2015.1010238.

Vázquez-Vargas, D.A. et al, 2020. Synthesis and microstructural characterization of cupric oxide and cobalt oxide nanostructures for their application as selective solar coatings. Thin Solid Films 706 (July 2019), 138046. https://doi.org/10.1016/j.tsf.2020.138046.

Xu, L. et al, 2022. Adsorption of micropollutants from wastewater using iron and nitrogen co-doped biochar: Performance, kinetics and mechanism studies. J. Hazard. Mater. https://doi.org/10.1016/j.jhazmat.2021.127606.

Xu, X., Chen, Z., Li, Y., Chen, W., Li, J., 2009. Surface Science Bulk and surfaceproperties of spinel Co3O4 by density functional calculations. Surf. Sci. 603, 653–658. https://doi.org/10.1016/j.susc.2008.12.036.

Yasin, Y., Hussein, M., Ahmad @ Amat, F., 2007. Adsorption of methylene blue onto treated activated carbon. Malaysian J Anal. Sci. 11 (2), 400–406.

Yu, X., Meng, Q., Luo, T., Jia, Y., Sun, B., Li, Q., Liu, J., Huang, X., 2013. Facet-dependent electrochemical properties of Co3O4 nanocrystals toward heavy metal ions. Sci. Rep. 3, 2886. https://doi.org/10.1038/srep02886.